Scientific Research Publishing

Open Journal of Applied Sciences, 2025, 15(3), 670-687
https://www.scirp.org/journal/ojapps
ISSN Online: 2165-3925
ISSN Print: 2165-3917

Optimal Design of Time-Delay Feedback Control in a Spring-Mass-Pendulum Vibration Reduction System

Jianwen Tu, Yanying Zhao, Changli Wang

School of Aircraft Engineering, Nanchang Hangkong University, Nanchang, China
Email: 454695810@qq.com

How to cite this paper: Tu, J.W., Zhao, Y.Y. and Wang, C.L. (2025) Optimal Design of Time-Delay Feedback Control in a Spring-Mass-Pendulum Vibration Reduction System. *Open Journal of Applied Sciences*, **15**, 670-687.
https://doi.org/10.4236/ojapps.2025.153043

Received: February 28, 2025
Accepted: March 17, 2025
Published: March 20, 2025

Abstract

This study investigates the application of time-delay feedback active control to the anti-resonant frequency response in a Pendulum Tuned Mass Damper (PTMD) vibration reduction system. An optimization method is proposed for controlling the anti-resonant frequency response in a time-delay-coupled mass-pendulum dynamic vibration absorber system. For systems with inherent damping in the primary structure, the time-delay feedback control is employed to optimize the anti-resonant frequency response while maintaining the overall vibration reduction performance of the primary system's amplitude-frequency response curve. First, the Cluster Treatment of Characteristic Roots (CTCR) method is applied to analyze the stability of the time-delay feedback control system, determining stable intervals for two critical parameters: time delay and feedback gain coefficient. Second, optimization criteria for the control system are established, and optimal control parameters are derived under these constraints. Finally, comparative studies with conventional models validate the effectiveness of the proposed control strategy.

Keywords

Anti-Resonant Frequency, Pendulum Tuned Mass Damper (PTMD), Time Delay, Active Control, Optimization Criteria

1. Introduction

Resonant and anti-resonant frequencies are critical indicators of dynamic characteristics in structural vibration systems, where the peaks and valleys in the frequency response spectrum correspond to these two characteristic frequencies, respectively. For systems incorporating a linear undamped dynamic vibration ab-

sorber (DVA), the amplitude of the primary system becomes zero at the anti-resonant frequency. This unique property underscores the significant engineering value of studying anti-resonant frequencies. As a specialized form of DVA, the pendulum tuned mass damper (PTMD) achieves energy transfer through vibrational coupling between the primary and auxiliary systems, thereby effectively suppressing vibrations in the primary system.

Scholars worldwide have conducted extensive research on parameter optimization and adjustment of PTMDs. Li Hongnan's team [1] [2] elucidated the influence laws of suspended mass-pendulum parameters on the tuning frequency ratio. Kwok *et al.* [3] developed a multi-linkage pendulum mechanism to address the long suspension requirements in building structures, while Hou Jie *et al.* [4] explored the effects of large-angle nonlinearity on frequency regulation. Notably, pendulum length adjustment, as a pivotal control mechanism, has been innovatively advanced in Zhang's [5] adaptive PTMD and He Haoxiang's [6] multi-pendulum synergistic tuning studies. In experimental validations, Dong Guohua *et al.* [7] successfully controlled multi-mode vibrations in cantilever beams through mass-ratio modulation, and Nagarajaiah's team [8] [9] demonstrated the efficacy of real-time pendulum-length adjustment in achieving frequency-adaptive technology.

To address the susceptibility of conventional PTMDs to parameter deviations, active control technologies have emerged as a promising trend. Christie *et al.* [10] achieved frequency dynamic regulation using a magnetorheological damper, while Hosek's team [11] [12] developed a centrifugal delayed resonator that broadens the control bandwidth through parameter self-adaptation. Since its inception by Olgac [13], time-delay feedback control theory has demonstrated significant potential in vibration suppression for both linear and nonlinear systems [14]-[17].

In this study, building upon Deraemaeker's model [18], we introduce the damping factor of the primary system for the first time and integrate it with time-delay feedback control for parameter optimization at the anti-resonant frequency. Theoretical derivations confirm that the proposed method effectively enhances the control performance of damped vibration systems, offering novel insights for engineering applications.

2. Mechanical Model and Vibration Differential Equations

The mechanical model of the time-delay coupled mass-pendulum vibration absorber system is shown in **Figure 1**.

The primary system can be simplified as a single-degree-of-freedom model with mass m_1, stiffness k_1, and damping c_1. $F(t) = f\cos(\omega t)$ represents the external excitation acting on the primary system, where f is the amplitude of the external excitation and ω is the frequency of the external excitation. The auxiliary system consists of a small ball with mass m_2 and negligible moment of inertia, which is connected to the center of gravity of the primary system by a rod of

length l with negligible mass. The secondary system can be simplified as a mass-spring-damper with mass m_2, stiffness k_2, and damping c_2.

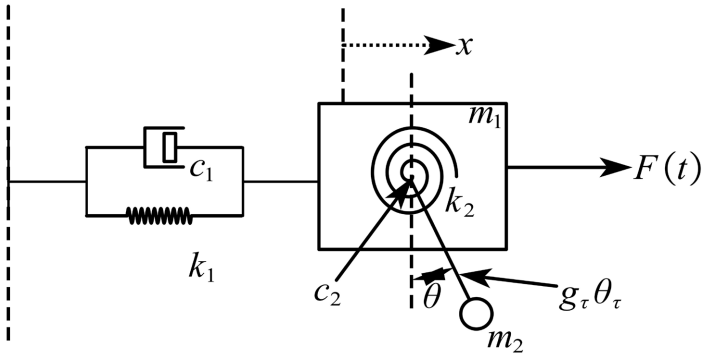

Figure 1. Mechanical model of delay-coupled pendulum tuned mass damper system.

The governing differential equations of the system are derived as follows:

$$m_1 x_0'' + k_1 x_0 + c_1 x_0' + m_2 \left(l\theta'' \cos\theta - l\theta'^2 \sin\theta + x_0'' \right) = f \cos(\omega t) \tag{1}$$

$$m_2 l^2 \theta'' + m_2 x_0'' l \cos\theta + c_2 \theta' + m_2 g_0 l \sin\theta + k_2 \theta + g_\tau \theta(t-\tau) = 0 \tag{2}$$

where $(') = \frac{\mathrm{d}}{\mathrm{d}t}, ('') = \frac{\mathrm{d}^2}{\mathrm{d}t^2}$, g_0 is the gravitational acceleration. Under the assumption of small angular displacement, the higher-order term θ'^2 becomes negligible. By $\sin\theta \approx \theta$ $\cos\theta \approx 1$, the original nonlinear governing equations (1)-(2) are linearized into the simplified system (3)-(4):

$$m_1 x_0'' + k_1 x_0 + c_1 x_0' + m_2 \left(l\theta'' + x_0'' \right) = f \cos(\omega t) \tag{3}$$

$$m_2 \left(l^2 \theta'' + x_0'' l + gl\theta \right) + c_2 \theta' + k_2 \theta + g_\tau \theta(t-\tau) = 0 \tag{4}$$

where $\theta(t-\tau) = \theta_\tau$, $g_\tau \theta_\tau$ represents the time-delay feedback control force. When, the time-delay feedback is disabled, and the system degenerates into a passive pendulum tuned mass damper (PTMD) vibration reduction system. To facilitate analysis, the following parameters and dimensionless quantities are introduced:

$$\mu = \frac{m_2}{m_1}, x = \frac{x_0}{l}, \omega_s = \sqrt{\frac{k_1}{m_1}}, \omega_p = \sqrt{\frac{k_2 + m_2 g_0 l}{m_2 l^2}},$$

$$\omega_q = \sqrt{\frac{g_\tau}{m_2 l^2}}, \alpha = \left(\frac{\omega_p}{\omega_s} \right)^2, g = \left(\frac{\omega_q}{\omega_s} \right)^2, \Omega = \frac{\omega}{\omega_s},$$

$$\xi_s = \frac{c_1}{2 m_1 \omega_s}, \xi_p = \frac{c_2 \omega_s}{2\left(k_2 + m_2 g_0 l \right)}, F = \frac{f}{m_1 \omega_s^2 l}, \tilde{t} = \frac{\omega}{\Omega} t, \tilde{\tau} = \frac{\omega}{\Omega} \tau.$$

For notational simplicity, the tilde (~) in the equations is omitted. The dimensionless forms of Equations (3)-(4) are expressed as:

$$(1+\mu)\ddot{x} + \mu\ddot{\theta} + 2\xi_s \dot{x} + x = F \cos(\Omega t) \tag{5}$$

$$\ddot{x} + \ddot{\theta} + 2\xi_p \alpha \dot{\theta} + \alpha\theta + g\theta_\tau = 0 \tag{6}$$

where $(\cdot)=\frac{\mathrm{d}}{\mathrm{d}\hat{t}},(\cdot\cdot)=\frac{\mathrm{d}^2}{\mathrm{d}\hat{t}^2}$

The steady-state solutions of Equations (5)-(6) can be represented in the following complex vector form: $x(t)=\Gamma \mathrm{e}^{i\omega t}$, $\theta(t)=\Theta \mathrm{e}^{i\omega t}$, where the external excitation term is denoted as $F\cos(\Omega t)=f\mathrm{e}^{i\omega t}$. Substituting these solutions into Equations (5)-(6) yields the amplitudes of the primary and auxiliary systems as:

$$\begin{bmatrix}\Gamma\\ \Theta\end{bmatrix}=\frac{F}{\Delta(\Omega)}\begin{bmatrix}\alpha+\mathrm{e}^{-i\Omega t}g-\Omega^2+2i\alpha\Omega\xi_p\\ \Omega^2\end{bmatrix} \tag{7}$$

where,

$$\Delta(\Omega)=-\mu\Omega^4+\left(\alpha+\mathrm{e}^{-i\Omega t}g-\Omega^2+2i\alpha\Omega\xi_p\right)\left[1-(1+\mu)\Omega^2+2i\Omega\xi_s\right] \tag{8}$$

The amplitude amplification factors for the primary system and the vibration absorber are respectively defined as:

$$h=\frac{\|\Gamma\|}{\tilde{F}},k=\frac{\|\Theta\|}{\tilde{F}} \tag{9}$$

where h and k represent the ratios of the response amplitudes to the external excitation force amplitude. The amplitude amplification factor h of the primary system, expressed as a function of the dimensionless excitation frequency Ω, is derived as follows:

$$\begin{aligned}h=&\left[\left(\alpha+g\cos(\Omega t)-\Omega^2\right)^2+\left(-g\sin(\Omega t)+2\alpha\Omega\xi_p\right)^2\right]^{1/2}\Big/\Big[\Big(-\mu\Omega^4\\&+\left(\alpha+g\cos(\Omega t)-\Omega^2\right)\left(1-(1+\mu)\Omega^2\right)-2\Omega\xi_s\left(-g\sin(\Omega\tau)\right.\\&\left.+2\alpha\Omega\xi_p\right)\Big)^2+\left(2\Omega\xi_s\left(\alpha+\cos(\Omega t)g-\Omega^2\right)\right.\\&\left.+\left(2\alpha\Omega\xi_p-g\sin(\Omega\tau)\right)\left(1-(1+\mu)\Omega^2\right)\right)^2\Big]^{1/2}\end{aligned} \tag{10}$$

3. CTCR Methodology and Stability Analysis Procedure

For a time-delay feedback control system, stability analysis must be performed to ensure stable operation. This process begins by deriving the characteristic equation of the governing Equations (3)-(4) as follows:

$$\begin{aligned}CE(s,g,\tau)=&s^4+\left(2\alpha\xi_p+2\alpha\mu\xi_p+2\xi_s\right)s^3\\&+\left(1+\alpha+\alpha\mu+g\theta_\tau+g\theta_\tau\mu+4\alpha\xi_s\xi_p\right)s^2\\&+\left(2\alpha\xi_p+2\alpha\xi_s+2g\theta_\tau\xi_s\right)s+\alpha+g\theta_\tau\end{aligned} \tag{11}$$

Since the vibration differential equations contain time-delay terms $\mathrm{e}^{-\lambda\tau}$, the characteristic equation (11) becomes a transcendental equation with exponential terms, possessing infinitely many characteristic roots. This study employs the Cluster Treatment of Characteristic Roots (CTCR) method [19] for stability analysis.

The CTCR stability analysis method plays a crucial and core role in the control strategy. Firstly, it provides an accurate quantitative evaluation method for system

stability. Through the clustering of system characteristic roots, it can clearly determine the stable states of the system under different combinations of time delays and feedback gain coefficients. This quantification process is not a simple data listing but a deep analysis of the internal dynamic characteristics of the system. It transforms the abstract concept of stability into a specific measurable parameter range, enabling researchers to have an intuitive and accurate understanding of system stability.

Secondly, CTCR provides a solid basis for the adjustment of control parameters. In the actual control process, reasonable time delays and feedback gain coefficients are crucial for achieving the optimal performance of the system. The stable range determined by CTCR through stability analysis guides researchers in optimizing parameters within this range. For example, in the Pendulum Tuned Mass Damper (PTMD) system, the time delay and feedback gain can be adjusted according to the CTCR results, enabling the system to maintain stability while effectively reducing the amplitude at the anti-resonance point and improving the overall vibration reduction performance. This precise parameter adjustment avoids blind attempts and greatly improves the efficiency and effectiveness of the control strategy.

Furthermore, the CTCR stability analysis method helps to highlight the advantages of the proposed control strategy compared with traditional methods. In traditional control models, there is often a lack of comprehensive and accurate quantitative analysis of system stability, making it difficult to ensure the stable operation and performance optimization of the system under complex working conditions. However, through its systematic analysis process, CTCR can not only ensure system stability but also open up new paths for system performance improvement at the theoretical level. Taking the time-delay feedback control method in this paper as an example, with the help of CTCR analysis, the potential of the system can be deeply explored theoretically, achieving a breakthrough over traditional control methods and bringing new solutions and ideas to fields such as structural vibration control.

The analytical procedure comprises the following steps:

1) Definition of Kernel Hypercurves (KH):

When the structural parameters of the system are fixed at specific values, a point in the two-dimensional (g,τ)-parameter plane that satisfies the condition of characteristic roots with zero real part $\lambda = j\Omega_c, \Omega_c \in \mathrm{R}^+$ is identified, and $0 \le \Omega_c \tau \le 2\pi$, $0 \le g \le 20$. The locus of all such qualifying points in the (g,τ)-parameter plane forms curves termed Kernel Hypercurves.

2) Definition of Offspring Hypercurves (OH):

The Offspring Hypercurves (OH) are generated from the aforementioned Kernel Hypercurves (KH) through the following nonlinear transformation (Equation (12)):

$$\left\{\tau + \frac{2\pi}{\Omega_c} i, g\right\}, i = 0,1,2,\cdots \tag{12}$$

3) Definition of Root Tendency (RT):

$$\mathrm{RT} = \mathrm{sgn}\left[\mathrm{Re}\left(\left.\frac{\partial\lambda}{\partial\tau}\right|_{\lambda=j\Omega_c}\right)\right] \tag{13}$$

Critical Time Delay $\tau_k \in (\tau_k - \nu, \tau_k + \nu), 0 < \nu \ll 1, k = 1,2,3,\cdots$: When $\mathrm{RT} = +1$: A pair of complex conjugate characteristic roots crosses the imaginary axis from the left-half plane (stable) to the right-half plane (unstable) in the (g,τ) -parameter plane. This transition increases the number of unstable roots by two as the time delay traverses τ_k from the left. When $\mathrm{RT} = -1$: Conversely, a pair of roots crosses from the right-half plane to the left-half plane, decreasing the number of unstable roots by two. In other time-delay intervals: The number of unstable roots remains constant.

Substitution via Euler's Formula:

$$\mathrm{e}^{-j\Omega_c\tau} = \cos(\psi_c) - j\sin(\psi_c),\ \psi_c = \Omega_c\tau \tag{14}$$

The cosine and sine functions are transformed into the following expressions using the half-angle identities of the tangent function:

$$\cos(\psi_c) = \frac{1-z_1^2}{1+z_1^2}, \sin(\psi_c) = \frac{2z_1}{1+z_1^2}, z_1 = \tan(\psi_c/2) \tag{15}$$

Subsequently, the system stability is analyzed based on the CTCR theory.

From Equations (14) and (15), the characteristic Equation (11) can be reformulated as a polynomial function in terms of Ω_c :

$$k(\Omega_c, g, z_1) = \sum_{k=0}^{4} \upsilon_k(g, z_1)(\Omega_c j)^k = 0 \tag{16}$$

where the coefficients υ_k are functions of g and z_1, and simultaneously act as coefficients of Ω_c .

By separating Equation (16) into real and imaginary parts and rearranging terms, we derive:

$$\mathrm{Re}\left[k(\Omega_c, g, z_1)\right] = \sum_{k=0}^{4} R_k(g, z_1)(\Omega_c)^k = 0 \tag{17}$$

$$\mathrm{Im}\left[k(\Omega_c, g, z_1)\right] = \sum_{k=0}^{4} I_k(g, z_1)(\Omega_c)^k = 0 \tag{18}$$

where R_k, I_k are coefficients associated with g, z_1, defined explicitly as follows:

$$\begin{cases} R_0 = g + \alpha - gz_1^2 + \alpha z_1^2 \\ R_1 = 4gz_1\xi_s \\ R_2 = -1 - g - \alpha - g\mu - \alpha\mu - z_1^2 + gz_1^2 - \alpha z_1^2 \\ \qquad + g\mu z_1^2 - \alpha\mu z_1^2 - 4\alpha\xi_p\xi_s - 4\alpha z_1^2\xi_p\xi_s \\ R_3 = 0 \\ R_4 = 1 + z_1^2 \end{cases} \tag{19}$$

$$\begin{cases} I_0 = -2gz_1 \\ I_1 = 2\alpha\xi_p + 2\alpha z_1^2\xi_p + 2g\xi_s + 2\alpha\xi_s - 2gz_1^2\xi_s + 2\alpha z_1^2\xi_s \\ I_2 = 2gz_1 + 2g\mu z_1 \\ I_3 = -2\alpha\xi_p - 2\alpha\mu\xi_p - 2\alpha z_1^2\xi_p - 2\alpha\mu z_1^2\xi_p - 2\xi_s - 2z_1^2\xi_s \\ I_4 = 0 \end{cases} \tag{20}$$

To solve for Ω_c from Equations (19) and (20), it is necessary to determine the necessary and sufficient conditions using the discriminant and Dixon resultant. The Dixon resultant provides a rigorous criterion for identifying non-trivial solutions of polynomial systems, and it exhibits superior accuracy compared to other resultant methods.

By applying the Dixon resultant, we set:

$$k_1(\Omega_c) \equiv \mathrm{Re}\left[k(\Omega_c, g, z_1)\right] \tag{21}$$

$$k_2(\Omega_c) \equiv \mathrm{Im}\left[k(\Omega_c, g, z_1)\right] \tag{22}$$

$$\delta(\Omega_c, \sigma) = \frac{1}{\Omega_c - \sigma}\begin{vmatrix} k_1(\Omega_c) & k_2(\Omega_c) \\ k_1(\sigma) & k_2(\sigma) \end{vmatrix} \tag{23}$$

where $k_1(\Omega_c)$ and $k_2(\Omega_c)$ are expressions obtained by substituting the auxiliary variable σ for Ω_c in Equations (21) and (22), as follows:

$$\begin{aligned} k_1(\Omega_c) = {} & \left(1+z_1^2\right)\Omega_c^4 + \left(-1-g-\alpha-g\mu-\alpha\mu-z_1^2+gz_1^2\right. \\ & \left.-\alpha z_1^2+g\mu z_1^2-\alpha\mu z_1^2-4\alpha\xi_p\xi_s-4\alpha z_1^2\xi_p\xi_s\right)\Omega_c^2 \\ & +4gz_1\xi_s\Omega_c+g+\alpha-gz_1^2+\alpha z_1^2 \end{aligned} \tag{24}$$

$$\begin{aligned} k_2(\Omega_c) = {} & \left(-2\alpha\xi_p-2\alpha\mu\xi_p-2\alpha z_1^2\xi_p-2\alpha\mu z_1^2\xi_p-2\xi_s-2z_1^2\xi_s\right)\Omega_c^3 \\ & +\left(2gz_1+2g\mu z_1\right)\Omega_c^2+\left(2\alpha\xi_p+2\alpha z_1^2\xi_p+2g\xi_s+2\alpha\xi_s\right. \\ & \left.-2gz_1^2\xi_s+2\alpha z_1^2\xi_s\right)\Omega_c-2gz_1 \end{aligned} \tag{25}$$

Expanding Equation (23) yields a symmetric $deg-1$ polynomial with respect to Ω_c and σ, referred to as the Dixon polynomial in terms of $q_1(\Omega_c)$ and $q_2(\Omega_c)$. Due to the symmetry of Equation (23), the positions of Ω_c and σ can be interchanged, leading to the equivalence $\delta(\Omega_c, \sigma) = \delta(\sigma, \Omega_c)$.

In the above context, deg denotes the highest degree of $k_1(\Omega_c)$ and $k_2(\Omega_c)$ with respect to Ω_c, *i.e.*, $deg = \max\left(deg\left(k_1(\Omega_c)\right), deg\left(k_2(\Omega_c)\right)\right)$, where $deg\left(k_1(\Omega_c)\right)$ and $deg\left(k_2(\Omega_c)\right)$ represent the highest degrees of Ω_c. Every common zero of $k_1(\Omega_c)$ and $k_2(\Omega_c)$ is also a zero of $\delta(\Omega_c, \sigma)$ for all values of σ. Consequently, under these common zeros, the coefficients of σ^i in $\delta(\Omega_c, \sigma)$ equate to zero, which can be expressed in matrix form as follows:

$$\boldsymbol{D}(g, z_1)\begin{pmatrix} 1 \\ \Omega_c \\ \vdots \\ \Omega_c^{deg-1} \end{pmatrix} = \begin{pmatrix} 0 \\ 0 \\ \vdots \\ 0 \end{pmatrix} \tag{26}$$

where $i = 0, 1, 2, \cdots, deg-1$ the coefficient matrix $\boldsymbol{D}(g, z_1) \in R^d$, constructed

from elements $d = deg \times deg$, is termed the Dixon matrix.

$$\boldsymbol{D}(g, z_1) = \begin{pmatrix} D_{11} & D_{12} & D_{13} & D_{14} \\ D_{21} & D_{22} & D_{23} & D_{24} \\ D_{31} & D_{32} & D_{33} & D_{34} \\ D_{41} & D_{42} & D_{43} & D_{44} \end{pmatrix} \tag{27}$$

where:

$$\begin{aligned} q_1 &= -1 + g - \alpha + g\mu - \alpha\mu - 4\alpha\xi_p\xi_s \\ q_2 &= 4g\xi_s \\ q_3 &= -g + \alpha \\ q_4 &= g + \alpha \\ q_5 &= -1 - g - \alpha - g\mu - \alpha\mu - 4\alpha\xi_p\xi_s \\ q_6 &= -2\alpha\xi_p - 2\alpha\mu\xi_p - 2\xi_s \\ q_7 &= 2g + 2g\mu \\ q_8 &= 2\alpha\xi_p - 2g\xi_s + 2\alpha\xi_s \\ q_9 &= 2\alpha\xi_p + 2g\xi_s + 2\alpha\xi_s \end{aligned}$$

$$\begin{aligned} D_{11} &= -q_3q_8z_1^4 - q_4q_8z_1^2 - q_3q_9z_1^2 - q_4q_9 \\ D_{12} &= -q_3q_7z_1^3 - q_4q_7z_1 \\ D_{13} &= -q_3q_6z_1^4 - q_3q_6z_1^2 - q_4q_6z_1^2 - q_4q_6 \\ D_{14} &= 0 \\ D_{21} &= -q_3q_7z_1^3 - q_4q_7z_1 \\ D_{22} &= -q_3q_6z_1^4 + q_1q_8z_1^4 - q_3q_6z_1^2 - q_4q_6z_1^2 - q_2q_7z_1^2 + q_5q_8z_1^2 + q_1q_9z_1^2 - q_4q_6 + q_5q_9 \\ D_{23} &= -q_2q_6z_1^3 - q_2q_6z_1 \\ D_{24} &= q_8z_1^4 + q_8z_1^2 + q_9z_1^2 + q_9 \\ D_{31} &= -q_3q_6z_1^4 - q_3q_6z_1^2 - q_4q_6z_1^2 - q_4q_6 \\ D_{32} &= -q_2q_6z_1^3 - q_2q_6z_1 \\ D_{33} &= -q_1q_6z_1^4 + q_8z_1^4 - q_1q_6z_1^2 - q_5q_6z_1^2 + q_8z_1^2 + q_9z_1^2 - q_5q_6 + q_9 \\ D_{34} &= q_7z_1^3 + q_7z_1 \\ D_{41} &= 0 \\ D_{42} &= q_8z_1^4 + q_8z_1^2 + q_9z_1^2 + q_9 \\ D_{43} &= q_7z_1^3 + q_7z_1 \\ D_{44} &= q_6z_1^4 + 2q_6z_1^2 + q_6 \end{aligned}$$

The necessary and sufficient condition for $q_1(\Omega_c)$ and $q_2(\Omega_c)$ to have common zeros is that the Dixon matrix $\boldsymbol{D}(g, z_1)$ is singular, *i.e.*,

$$Det\left[\boldsymbol{D}(g, z_1)\right] = 0 \tag{28}$$

If g is constrained within a prescribed interval, the Dixon matrix $Det\left[\boldsymbol{D}(g, z_1)\right] = 0$ reduces to a 16th-degree polynomial in z_1:

$$\Delta_{z_1} = \sum_{k=0}^{16} \phi_K(g) z_1^k = 0 \tag{29}$$

where $\phi_K(g)$ denotes the coefficients of z_1 at various orders. Due to their complexity, these coefficients are not explicitly listed here.

The stable regions for the time-delay feedback gain coefficient g and time-delay parameter τ are determined through the following analytical steps:

1) Fix the feedback gain coefficient g, compute the roots of the polynomial equation (29), and substitute the real roots into the trigonometric expression (15).

2) Calculate $v_c = \Omega_c \tau_c$ from expression (15), substitute it into (14) to obtain Ω_c, and then substitute $e^{-j\Omega_c \tau}$ into the characteristic equation (11) to compute all characteristic roots.

3) From the computed characteristic roots, identify the purely imaginary roots. The corresponding frequencies are termed critical crossing frequencies, denoted as Ω_c.

4) Substitute Ω_c into Equation (14) to solve for $\tau_{ci}, i = 1, 2, 3, \cdots$

5) Investigate system stability within the studied parameter range $K_0 = \{(g, \tau) \mid 0 \le g \le 2.0, 0 \le \tau \le 2.0\}$: incrementally vary the feedback gain coefficient from 0 to 2.0, repeat steps (1)-(4), and determine the stable control parameter region $K_1 = \{(g, \tau) \mid \mathrm{Re}[CE(p, g, \tau)] < 0\} \cap \{(g, \tau) \mid 0 \le g \le 2.0, 0 \le \tau \le 2.0\}$. Other fixed structural parameters include: $p = \{\mu, \xi_s, \xi_p, \alpha\} = \{0.1, 0.312, 0.502, 0 \sim 2.0\}$.

4. Amplitude Optimization Criterion at Anti-Resonance Points

Building upon the governing Equations (5)-(6), this study implements an optimization control strategy for anti-resonance point amplitudes by introducing a time-delay feedback active control mechanism. The anti-resonance phenomenon is mathematically characterized by the minimum amplitude state of the primary system described in Equation (9). This extremum property exhibits a strict correspondence with the minima of the solutions to Equations (5)-(6). Based on function extremum theory, the mathematical conditions for the anti-resonance point must satisfy the following criteria:

$$\frac{\mathrm{d}A_1}{\mathrm{d}\Omega} = 0, \frac{\mathrm{d}^2 A_1}{\mathrm{d}\Omega^2} > 0 \tag{30}$$

This study addresses a two-degree-of-freedom linear system, where the minimum amplitude condition of the primary system also corresponds to the criteria for determining the anti-resonance point. First, the anti-resonance frequency is derived from Equation (30). Substituting this frequency into the primary system's amplitude expression (Equation (9)) yields the amplitude at the anti-resonance point. Then, under fixed structural parameters of the vibration system ($p = \{\mu, \xi_s, \xi_p, \alpha\}$), the feedback gain coefficient and time delay are adjusted to control the amplitude at the anti-resonance point within a specified range, *i.e.* $\min \|A_1(p, \Omega_a, g, \tau)\| < H_{anti}$. The proposed optimization criterion for minimizing the amplitude at the anti-resonance point is as follows:

$$\begin{aligned} &\left.\frac{\mathrm{d}A_1}{\mathrm{d}\Omega}\right|_{\Omega=\Omega_a} = 0 \\ &\left.\frac{\mathrm{d}^2A_1}{\mathrm{d}\Omega^2}\right|_{\Omega=\Omega_a} > 0 \\ &\min\left\|A_1\left(p,\Omega_a,g,\tau\right)\right\| < H_{anti} \end{aligned} \tag{31}$$

In the above equation, H_{anti} represents the maximum amplitude of the primary system at the anti-resonance point, $\min\left\|A_1\left(p,\Omega_a,g,\tau\right)\right\| < H_{anti}$ denotes the specified threshold that the anti-resonance amplitude must not exceed (*i.e.*, H_{anti}), $A_1\left(p,\Omega_a,g,\tau\right)$ is the amplitude at the anti-resonance point, and Ω_a is the frequency of the anti-resonance point. This study employs $H_{anti}=0.1$ as an example for optimization calculations.

K_2 is defined as the operational range of feedback gain coefficients and time delays that simultaneously satisfy two conditions: 1) stability of the system and 2) the amplitude minimization criterion at the anti-resonance point. It is formulated as follows:

$$\begin{aligned} K_2 = &\left\{\left(g,\tau\right)\middle|\min\left\|A_1\left(p,\Omega_a,g,\tau\right)\right\| < 0.01\right\} \\ &\cap\left\{\left(g,\tau\right)\middle|\mathrm{Re}\left[CE\left(p,g,\tau\right)\right] < 0\right\} \end{aligned} \tag{32}$$

First, initialize the optimization parameters for the vibration system as follows:

$$p_0 = \left\{\mu,\xi_s,\xi_p,\alpha\right\} = \left\{0.1, 0.312, 0.185, 0\sim 2\right\} \tag{33}$$

The structural parameters between p_0 and p are divided into N equal intervals, with the optimization step size denoted as $\Delta p = \left(p_0 - p\right)/N$. A larger N corresponds to a smaller Δp, yielding higher precision. Here, $N=100$. The structural parameters μ,ξ_s,ξ_p,α remain unchanged, while the value of α spans from p_0 to p. At the $h+1$-th step, the structural parameters are set as $p_{h+1} = p_h + \Delta p$, where p_h represents the structural parameters at the h-th iteration.

Finally, after completing the stepwise incremental adjustment of the structural parameter p_{h+1}, substitute the parameter values from each step into Equations (31) and (32) to determine the operational regions for the feedback gain coefficient g and time delay τ. The iterative computation workflow is illustrated in Figure 2.

5. Stability Analysis and Optimization Effectiveness

Figure 3 displays a three-dimensional surface plot, where each point on the surface represents a stable configuration of the vibration system. As shown in the figure, as the structural optimization coefficient α increases, the stability regions generally decrease in size.

Figure 4 (specific case): For a fixed value of the structural optimization coefficient α, the curve shows stable system configurations. Key observations: At a constant feedback gain coefficient g, a smaller α requires a larger τ to

maintain stability. At a constant time delay τ, a smaller α corresponds to a feedback gain coefficient g that first decreases and then increases to achieve stability.

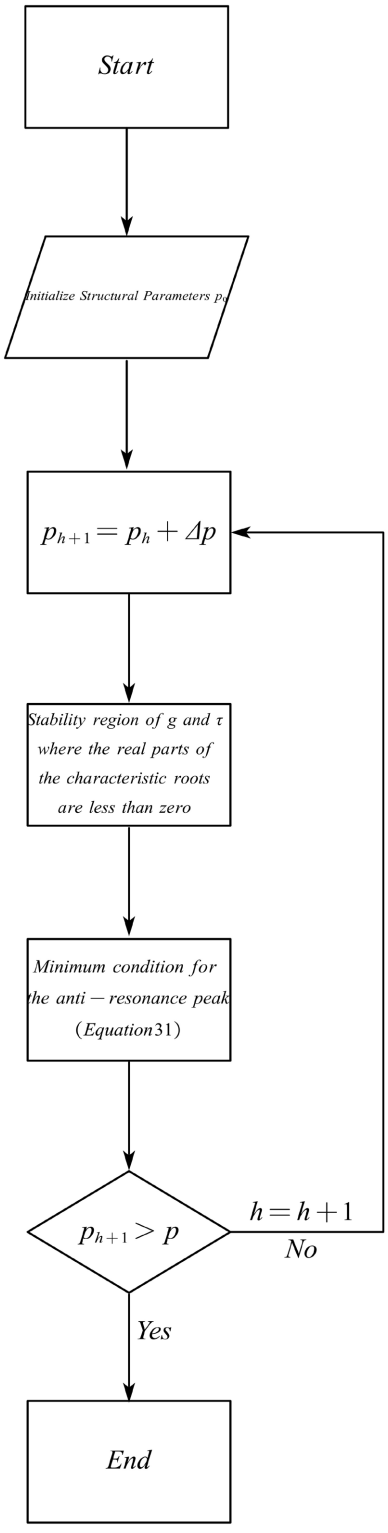

Figure 2. The iterative computation workflow.

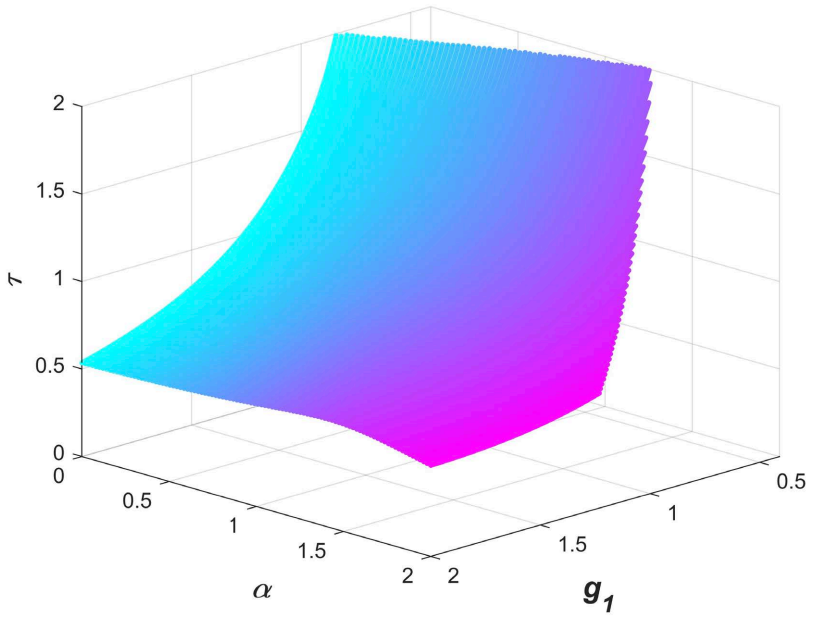

Figure 3. Stability regions for structural optimization coefficient, feedback gain coefficient, and time delay.

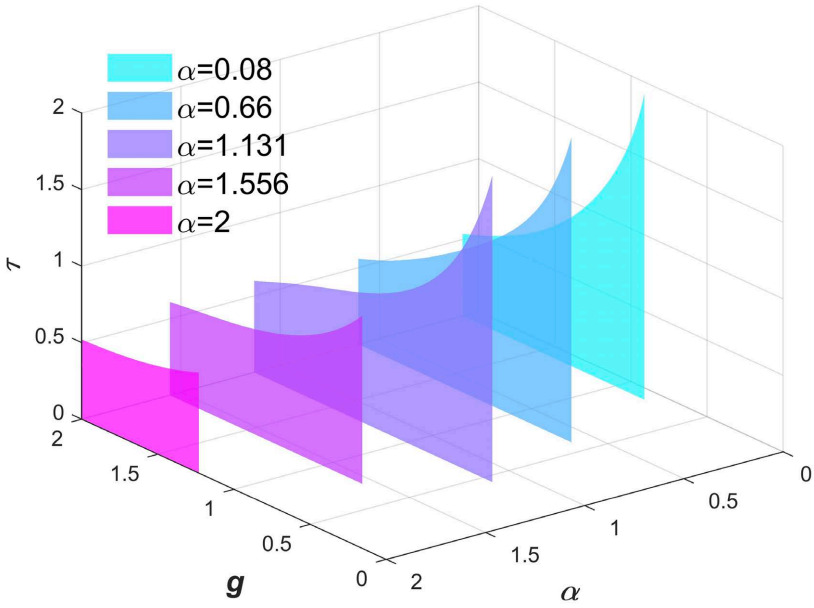

Figure 4. Stability regions of feedback gain coefficient and time delay under different structural optimization coefficients.

Figure 5 illustrates the relationship between the controlled anti-resonance frequency range (via adjustments of g and τ) and the corresponding primary system amplitude at the anti-resonance point under different structural optimization coefficients α.

- Upper plane: Vertical axis represents the feedback gain coefficient g.
- Lower plane: Vertical axis represents the amplitude of the primary system at the anti-resonance point.

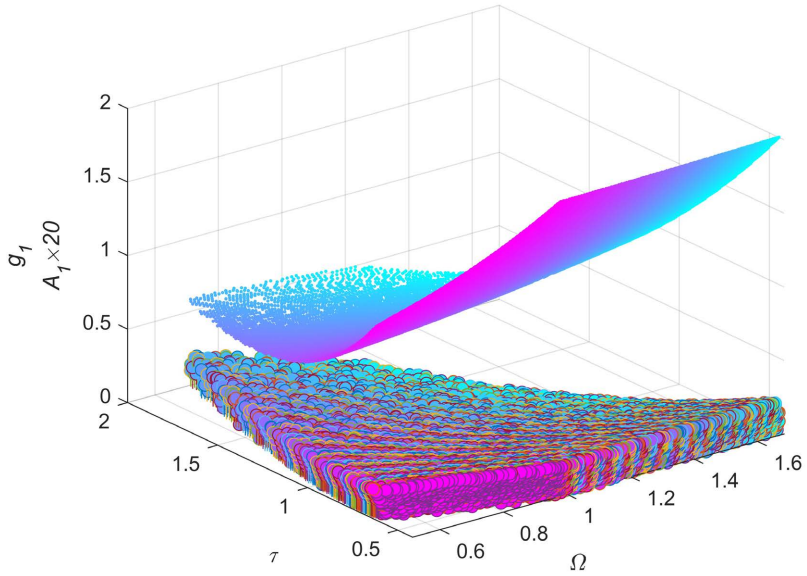

Figure 5. Response of feedback gain coefficient -time delay (primary system anti-resonance amplitude).

To clarify the correspondence between the anti-resonance frequency Ω, feedback gain coefficient g, and structural optimization coefficient α, five values of α are analyzed: 0, 0.45, 0.90, 1.35, 1.75 (as shown in **Figure 6**).

- Triangular markers: Curves represent the feedback gain coefficient g.
- Circular markers: Curves represent the amplitude at the anti-resonance point of the primary system.

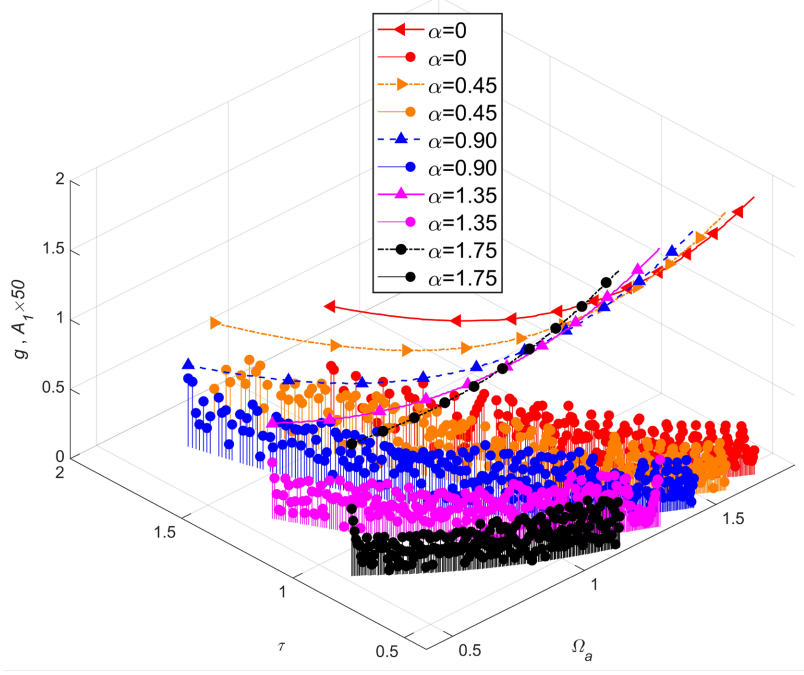

Figure 6. Response of feedback gain coefficient-time delay (primary system anti-resonance amplitude) under different structural optimization coefficients.

From Figure 6, it can be observed that there exists a series of adjustment ranges for the feedback gain coefficient g and time delay τ that satisfy the constraints on the anti-resonance amplitude. As shown in Figure 6: As g increases, the time delay τ gradually decreases. As α increases, the adjustment ranges for g and τ meeting the anti-resonance amplitude optimization criteria continuously shrink. Increasing τ shifts the anti-resonance frequency toward lower frequencies. Increasing α also shifts the anti-resonance frequency toward lower frequencies.

From Figure 7: Anti-resonance frequency ranges under different structural optimization coefficients α. To clarify the tunable anti-resonance frequency band, Figure 7 illustrates the following:

- Ω_L : Minimum anti-resonance frequency.
- Ω_H : Maximum anti-resonance frequency.
- $\Omega = \omega/\omega_1 = 1$: Primary resonance frequency (external excitation frequency equals the natural frequency of the primary system).

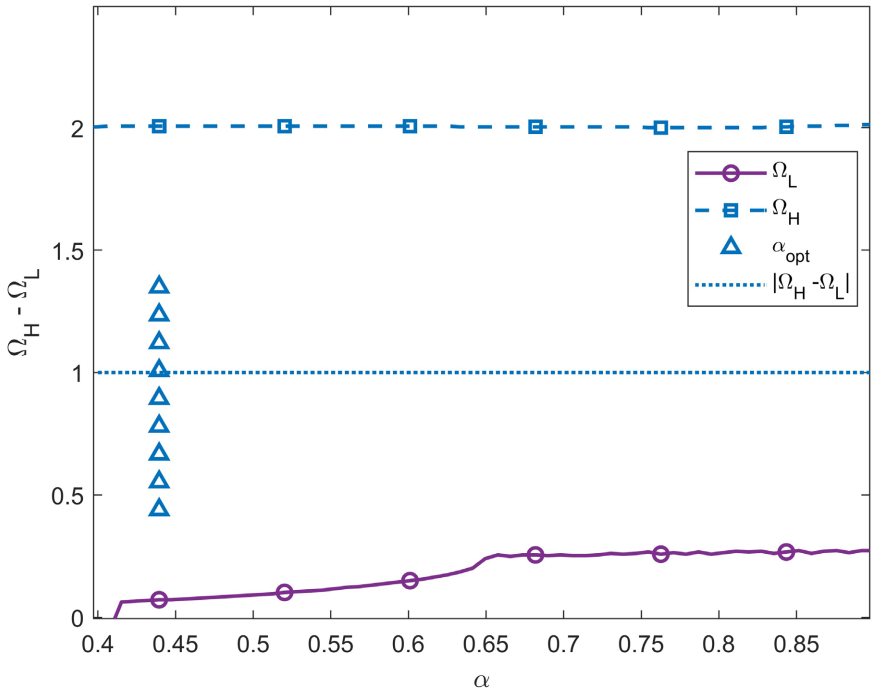

Figure 7. Anti-resonance frequency ranges under different structural optimization coefficients.

From Figure 7, the following observations can be made: As the structural optimization coefficient α increases, the maximum anti-resonance frequency remains almost unchanged. The minimum anti-resonance frequency initially increases and then exhibits a gradual, slow rise.

The analysis reveals the existence of an optimal structural optimization coefficient α_{opt}, defined such that: The tunable range of anti-resonance frequencies achieves its maximum. The anti-resonance frequency band exhibits excellent sym-

metry around the primary resonance point, with frequencies approximately uniformly distributed on both sides. Thus, the optimal structural optimization coefficient is selected as $\alpha_{opt} = 0.439$. The corresponding optimal structural parameters of the system are determined as follows: $\mu = 0.1$, $\xi_{1opt} = 0.312$, $\xi_{2opt} = 0.185$, $\alpha_{opt} = 0.439$.

6. Comparative Validation of Anti-Resonance Frequency Control Effectiveness

To validate the amplitude optimization effectiveness at the anti-resonance frequency achieved by the proposed method, Figure 8 compares the amplitude-frequency response curves of the primary system with three vibration absorbers. Purple curve represents the classical two-degree-of-freedom (2-DOF) dynamic vibration absorber (DVA) studied by Asami [20]. Red curve represents the passive negative-stiffness dynamic vibration absorber with an amplification mechanism investigated by Peng [21]. Green curve represents the optimized results from this study.

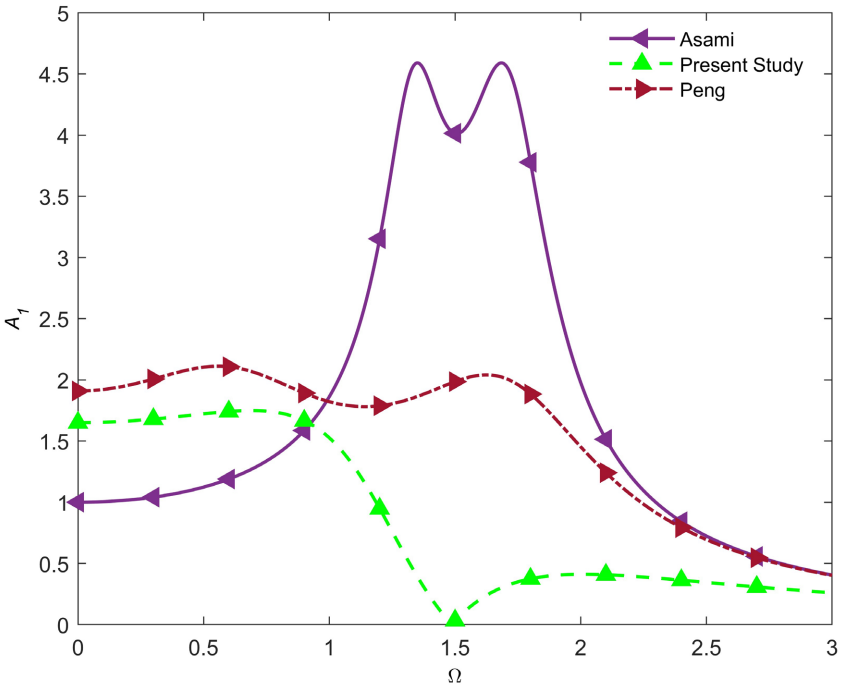

Figure 8. Amplitude-frequency response curves under different dynamic vibration absorber models.

The time-delay-controlled dynamic vibration absorber system proposed in this study demonstrates significant advantages in regulating system dynamic characteristics through coordinated optimization of feedback gain coefficients and time-delay parameters. Notably, under anti-resonance conditions, the vibration response of the primary structure is effectively suppressed to its theoretical minimum. Compared to the classical dynamic vibration absorber designed by Asami

and the passive negative-stiffness dynamic vibration absorber with an amplification mechanism studied by Peng, the proposed system achieves superior vibration suppression across the entire frequency range.

7. Conclusions

1) After performing equal-peak optimization on the passive control system with a spring-mass pendulum dynamic vibration absorber, the amplitude of the primary system remained relatively large. Therefore, time-delay feedback control technology was introduced to further control the amplitude of the primary system.

2) The CTCR method was used to partition the stability regions of the time-delay feedback control system, obtaining stable operating regions for the feedback gain coefficient and time delay.

3) The influence of the structural optimization coefficient on anti-resonance frequencies was analyzed: as the structural optimization coefficient gradually increases, the anti-resonance frequency shifts toward lower frequencies. The maximum anti-resonance frequency remains almost unchanged, while the minimum anti-resonance frequency initially increases and then rises slowly. An optimal structural optimization coefficient exists, maximizing the tunable range of anti-resonance frequencies and ensuring symmetric distribution of the anti-resonance band relative to the primary resonance point.

4) By adjusting the feedback gain coefficient and time delay of the time-delay feedback control system, the amplitude at the anti-resonance point is effectively suppressed, almost completely eliminating the amplitude at the anti-resonance point.

Funding

Supported by the National Natural Science Foundation of China (12072140).

Conflicts of Interest

The authors declare no conflicts of interest regarding the publication of this paper.

References

[1] Li, H.N. and Singh, M.P. (1994) Optimum Parameters of Vibration Energy Dissipating Pendulum for Structures. *World Earthquake Engineering*, **11**, 14-17.

[2] Li, H.N. (1996) Study on Vibration Damping Properties of Pendulum-Structure System. *Engineering Mechanics*, **13**, 123-129.

[3] Kwok, K.C.S. and Samali, B. (1995) Performance of Tuned Mass Dampers under Wind Loads. *Engineering Structures*, **17**, 655-667. https://doi.org/10.1016/0141-0296(95)00035-6

[4] Hou, J., Huo, L.S. and Li, H.N. (2014) Research on Seismic Control of Transmission Towers with Nonlinear Suspending Mass Pendulum. *Journal of Vibration and Shock*, **33**, 177-181.

[5] Shu, Z., Li, S., Zhang, J. and He, M. (2017) Optimum Seismic Design of a Power Plant

Building with Pendulum Tuned Mass Damper System by Its Heavy Suspended Buckets. *Engineering Structures*, **136**, 114-132. https://doi.org/10.1016/j.engstruct.2017.01.010

[6] He, H.X., Xu, H.G. and Xu, W.B. (2019) Dynamic Characteristics Analysis of Suspended Double Pendulum and Its Application in Structural Vibration Reduction Control. *Journal of Vibration Engineering*, **32**, 305-313. https://doi.org/10.16385/j.cnki.issn.1004-4523.2019.02.014

[7] Dong, G.H., Yuan, G.Q. and Wang, B.X. (2007) Experimental Design of Mass Pendulum Vibration Damping Structure. *Mechanics in Engineering*, **29**, 3.

[8] Nagarajaiah, S. and Sonmez, E. (2007) Structures with Semiactive Variable Stiffness Single/Multiple Tuned Mass Dampers. *Journal of Structural Engineering*, **133**, 67-77. https://doi.org/10.1061/(asce)0733-9445(2007)133:1(67)

[9] Nagarajaiah, S. and Pasala, D.T.R. (2010) NEESR-Adapt-Struct: Semi-Active Control of ASD Device—Adaptive Length Pendulum Dampers. *Proceedings of the* 19*th Analysis and Computation Specialty Conference*, 325-334. https://doi.org/10.1061/41131(370)28

[10] Christie, M.D., Sun, S., Deng, L., Ning, D.H., Du, H., Zhang, S.W., *et al.* (2019) A Variable Resonance Magnetorheological-Fluid-Based Pendulum Tuned Mass Damper for Seismic Vibration Suppression. *Mechanical Systems and Signal Processing*, **116**, 530-544. https://doi.org/10.1016/j.ymssp.2018.07.007

[11] Hosek, M., Elmali, H. and Olgac, N. (1997) Centrifugal Delayed Resonator: Theory and Experiments. *ASME* 1997 *Design Engineering Technical Conferences*, Sacramento, 14-17 September 1997, V01BT08A006. https://doi.org/10.1115/detc97/vib-3829

[12] Hosek, M., Olgac, N. and Elmali, H. (1999) The Centrifugal Delayed Resonator as a Tunable Torsional Vibration Absorber for Multi-Degree-of-Freedom Systems. *Journal of Vibration and Control*, **5**, 299-322. https://doi.org/10.1177/107754639900500209

[13] Olgac, N. and Holm-Hansen, B.T. (1994) A Novel Active Vibration Absorption Technique: Delayed Resonator. *Journal of Sound and Vibration*, **176**, 93-104. https://doi.org/10.1006/jsvi.1994.1360

[14] Zhao, Y. and Xu, J. (2007) Effects of Delayed Feedback Control on Nonlinear Vibration Absorber System. *Journal of Sound and Vibration*, **308**, 212-230. https://doi.org/10.1016/j.jsv.2007.07.041

[15] Xu, J. and Sun, Y. (2015) Experimental Studies on Active Control of a Dynamic System via a Time-Delayed Absorber. *Acta Mechanica Sinica*, **31**, 229-247. https://doi.org/10.1007/s10409-015-0411-z

[16] Sun, X., Xu, J., Wang, F. and Cheng, L. (2019) Design and Experiment of Nonlinear Absorber for Equal-Peak and De-Nonlinearity. *Journal of Sound and Vibration*, **449**, 274-299. https://doi.org/10.1016/j.jsv.2019.02.033

[17] Wang, F., Sun, X., Meng, H. and Xu, J. (2021) Time-Delayed Feedback Control Design and Its Application for Vibration Absorption. *IEEE Transactions on Industrial Electronics*, **68**, 8593-8602. https://doi.org/10.1109/tie.2020.3009612

[18] Deraemaeker, A. and Soltani, P. (2016) A Short Note on Equal Peak Design for the Pendulum Tuned Mass Dampers. *Proceedings of the Institution of Mechanical Engineers*, *Part K*: *Journal of Multi-Body Dynamics*, **231**, 285-291. https://doi.org/10.1177/1464419316652558

[19] Fazelinia, H., Sipahi, R. and Olgac, N. (2007) Stability Robustness Analysis of Multiple Time-Delayed Systems Using "Building Block" Concept. *IEEE Transactions on*

Automatic Control, **52**, 799-810. https://doi.org/10.1109/tac.2007.898076

[20] Asami, T. and Nishihara, O. (2003) Closed-Form Exact Solution to H∞ Optimization of Dynamic Vibration Absorbers (Application to Different Transfer Functions and Damping Systems). *Journal of Vibration and Acoustics*, **125**, 398-405. https://doi.org/10.1115/1.1569514

[21] Peng, H.B., Shen, Y.J. and Yang, S.P. (2015) Parameter Optimization of a Novel Dynamic Vibration Absorber with Negative Stiffness Elements. *Chinese Journal of Theoretical and Applied Mechanics*, **47**, 320-327.